J Mater Sci (2021) 56:9644–9654

Ceramics

Investigating hollandite–perovskite composite ceramics as a potential waste form for immobilization of radioactive cesium and strontium

Jiang Ma[1], Zhiwei Fang[1], Xiaoyong Yang[1,2], Bo Wang[1], Fen Luo[1], Xiaoli Zhao[1], Xiaofen Wang[1], and Yushan Yang[1,*]

[1] *Fundamental Science on Nuclear Wastes and Environmental Safety Laboratory, Southwest University of Science and Technology, Mianyang 621010, China*

[2] *Condensed Matter Theory Group, Materials Theory Division, Department of Physics and Astronomy, Uppsala University, Box 516, 75120 Uppsala, Sweden*

Received: 29 November 2020
Accepted: 3 February 2021
Published online: 22 February 2021

ABSTRACT

Ceramic matrix containing zirconolite, hollandite, and perovskite phases is proposed as a potential host for HLW immobilization. Hollandite phase principally immobilizes Cs, while perovskite phase mainly immobilizes Sr. In this study, hollandite–perovskite composite ceramics are considered as a specialized waste form for immobilizing the separated Cs and Sr from HLW streams and synthesized by a solid-state reaction method at 1300 °C for 5 h. The phase compositions of the synthesized composites were characterized by XRD and BSE. The XRD results indicated that the as-prepared ceramics are composed of tetragonal hollandite $Ba_{0.8}Cs_{0.4}Al_2Ti_6O_{16}$, cubic perovskite $SrTiO_3$, alongside a lesser amount of TiO_2. The BSE—EDX results confirm that Cs partitions into the hollandite matrix, while Sr incorporates into perovskite host with homogenous distribution. In addition, aqueous durability testing was carried out using the MCC-1 static leach test method. The normalized release rates of Cs and Sr in HP-3 sample (i.e., 75 wt% $Ba_{0.8}Cs_{0.4}Al_2Ti_6O_{16}$ + 25 wt% $SrTiO_3$) were $< 10^{-2}$ $g{\cdot}m^{-2}{\cdot}d^{-1}$ after 42 days, exhibiting excellent chemical durability. These results indicate that the hollandite–perovskite ceramic matrix could be considered as a customized host matrix for immobilization of the separated Cs and Sr from HLW streams.

Handling Editor: M. Grant Norton.

Jiang Ma and Zhiwei Fang are co-first authors.

Address correspondence to E-mail: yys168994@126.com

https://doi.org/10.1007/s10853-021-05886-2

Introduction

Disposal of radioactive wastes, especially high-level nuclear wastes (HLW) produced during the reprocessing of spent nuclear fuels [1, 2], is still a challenging task because of their high radiotoxicity [3–6]. Until now, borosilicate glass is the only waste form applied at the industrial scale [7, 8]. Due to superior stable nature, ceramic waste form materials may improve the long-term aqueous performance in the disposal environment, relative to vitrified matrices [9, 10]. In order to properly dispose of the radioactive hazards and diminish their effects on the environment, crystalline ceramics have been regarded as a potential nuclear host to immobilize HLW [11–14]. On the atomic-scale, the radioactive waste elements are usually incorporated into the lattices structure of Synroc mineral phases, which would provide a more secure immobilization barrier compared with that in nuclear glasses. Previous results indicated that the normalized release rates of Cs, Sr, Ca and U in ceramic waste form are $\sim 7.8 \times 10^{-3}$, 7.0×10^{-4}, 8.0×10^{-3}, $< 10^{-4}$ $g{\cdot}m^{-2}{\cdot}d^{-1}$ respectively, which is $2 \sim 3$ orders of magnitude lower than that of 1.03, 7.5×10^{-2}, 6.8×10^{-2}, 0.1 $g{\cdot}m^{-2}{\cdot}d^{-1}$ in borosilicate glass [15–17]. In addition, ^{238}Pu-doped Synroc-C remains primary crystalline matrix for cumulative radiation doses of 10^{19} alpha/g [18], illustrating ceramic waste form is a satisfactory host for HLW.

Cesium (Cs) and strontium (Sr) are two of the major fission products and commonly exist in the nuclear waste stream from the reprocessing of spent fuels and primarily responsible for the heat generation in the storage system during the first few centuries [19, 20]. As two major concerned fission products for disposal of HLW, separation of Cs and Sr from spent nuclear fuel will reduce the nuclear waste volumes and radioactivity of HLW, which can simplify waste-handling operations and reduce the thermal load of the HLW storage [21, 22]. Due to high toxicity and solubility, the separated Cs and Sr must be immobilized in a robust host for final disposal. Previous results demonstrated that hollandite—type are of great interest to act as a host for Cs, while perovskite matrices are suitable to host Sr [23–25]. The general formula of hollandite is $A_xB_yC_{8-y}O_{16}$ ($x \leq 2$), A-sites are occupied by the large ions (i.e., Cs^+, Ba^{2+}, Rb^+), while small cations (i.e., Mg^{2+}, Al^{3+}, Ti^{4+}, Fe^{3+} and Sb^{5+}) are located at the B and C-site. In $A_xB_yC_{8-y}O_{16}$, the hollandite structure comprises corner and edge-sharing BO_6 and CO_6 octahedra forming tunnels along the c-axis, and the large A-site ions are located in these tunnels [26]. In perovskite (ABO_3), BO_6 octahedra share corners to form a 3D framework with large central cavities, the A cations are located in these cavities [27]. The naturally mineral of perovskite is $CaTiO_3$, which is easy to incorporate Sr in the perovskite structure due to the similar ionic and the similar chemistry of Ca and Sr. Importantly, in SYNROC-C, hollandite and perovskite phases are specifically targeted to accommodate Cs and Sr, respectively [28]. Thus, hollandite–perovskite composite ceramics are expected to be an excellent host matrix for final disposal of Cs and Sr.

Motivated by merits of hollandite-type ceramics and perovskite matrices above, we developed a hollandite–perovskite ceramic waste form for immobilization of Cs and Sr simultaneously. The $Ba_{0.8}Cs_{0.4}Al_2Ti_6O_{16}$—$SrTiO_3$ assemblage was synthesized in our work by a solid-state reaction method. The phase composition, microstructure and chemical durability of the as-prepared ceramic waste form were systemically investigated.

Experimental

Synthesis of hollandite–perovskite ceramics

The hollandite–perovskite composite ceramics were designed and synthesized to immobilize Cs and Sr. The nominal phase compositions are: 85 wt%, 80 wt%, 75 wt%, 70 wt%, 65 wt%, and 60 wt% for $Cs_{0.4}Ba_{0.8}Al_2Ti_6O_{16}$, and 15 wt%, 20 wt%, 25 wt%, 30 wt%, 35 wt% and 40 wt% for $SrTiO_3$ (named them as HP-1, HP-2, HP-3, HP-4, HP-5, and HP-6). In a typical process, Analytical Reagent (AR) starting materials of Cs_2CO_3 (99% purity, Aladdin Co. Ltd.), $BaCO_3$ (99% purity, Aladdin Co. Ltd.), $SrCO_3$ (99% purity, Aladdin Co. Ltd.), Al_2O_3 (98% purity, Aladdin Co. Ltd.) and TiO_2 (99% purity, mixture of rutile and anatase, Aladdin Co. Ltd.) are used to prepare samples. All initial powders are pre-heated at 120 °C for 2 h in order to remove adsorbed water. The dried powders were prepared according to Table 1 and sufficiently homogenized by the agate mortar and pestle in ethyl alcohol media for 2 h. The homogenized mixtures were dried and pressed into pellets (12 mm in diameter and 3 mm in thickness) at a

Table 1 Contents of the raw reactants in the designed hollandite–perovskite ceramics (H = $Ba_{0.8}Cs_{0.4}Al_2Ti_6O_{16}$; P = $SrTiO_3$)

Sample	Composition	Cs_2CO_3(g)	$BaCO_3$(g)	$SrCO_3$(g)	Al_2O_3(g)	TiO_2(g)
HP-1	85 wt% H + 15 wt% P	0.4372	1.0590	0.7241	0.6840	3.6068
HP-2	80 wt% H + 20 wt% P	0.4115	0.9967	0.9655	0.6438	3.5483
HP-3	75 wt% H + 25 wt% P	0.3857	0.9344	1.2069	0.6036	3.4897
HP-4	70 wt% H + 30 wt% P	0.3600	0.8721	1.4482	0.5633	3.4312
HP-5	65 wt% H + 35 wt% P	0.3343	0.8098	1.6896	0.5231	3.3727
HP-6	60 wt% H + 40 wt% P	0.3086	0.7475	1.9309	0.4829	3.3141

pressure of 12 MPa. To explore an optimum sintering temperature, a representative HP-3 sample (i.e., 75 wt% $Ba_{0.8}Cs_{0.4}Al_2Ti_6O_{16}$ + 25 wt% $SrTiO_3$) was chosen and sintered at 1200–1350 °C for 5 h in ambient atmosphere, with heating rate of 10 °C/min. After that, the compacted HP-1 ~ 6 pellets were sintered at the optimum sintering temperature.

Characterization

Simultaneous thermogravimetry and differential scanning calorimetry (TG-DSC, SDT Q600) was used to investigate the thermal behavior of hollandite–perovskite ceramic from room temperature to 1350 °C with a heating rate of 10 °C/min and 100 mL/min air flow. The crystalline phases of the sintered ceramics were characterized by X-ray diffraction (XRD, X'Per PRO, Netherlands) with Cu Kα radiation (λ = 1.5406 Å). The data were collected at 2 θ = 10 ~ 90° with step size of 0.02°. The General Structure Analysis System (GSAS) program was employed to obtain the lattice parameters of targeted hollandite and perovskite matrices in the synthesized materials [29]. The refinements proceeded as follows: the initial structural model for the $Ba_{0.8}Cs_{0.4}Al_2Ti_6O_{16}$, $SrTiO_3$ and TiO_2 Rutile were taken from the crystallographic data of $Cs_{0.187}Ba_{0.965}Al_{2.115}Ti_{5.885}O_{16}$ (JCPDS card no. 78–0018, space group *I*4/m), $SrTiO_3$ (JCPDS card no. 35–0734, space group *Pm* $\bar{3}$*m*) and TiO_2 (JCPDS card no. 73–1765, space group *P*42/*mnm*). At the beginning of refinements, the scale factor and background were firstly converged, then the lattice parameters and phase fraction were added and refined. Final, the peak profiles were fitted to pseudo-Voigt convolution functions. On convergence of the preceding parameters, the atomic coordinates and atomic isotropic temperature factors were also refined. The sintered HP-3 sample, as a representative of the sintered pellets was selected to investigate phase distribution and aqueous durability of hollandite–perovskite ceramics. The HP-3 sample was polished by metallographic sandpaper to a roughness of ~ 1 μm. The phase distribution of the polished HP-3 sample was studied using backscattering electron (BSE, Ultra55, Zeiss). Energy-dispersive X-ray spectroscopy (EDX, IE450X-Max80, Oxford) attached to the BSE equipment was used to collected elemental maps from multiphase regions and identify chemical composition of the targeted hollandite and perovskite matrices.

A leaching test was carried out using the static leach test (Materials Characterization Center, MCC-1) method [30]. The sample HP-3 was suspended in the closed Teflon container with deionized water. The sealed vessels were then placed in an oven maintained at 90 ± 2 °C for a period of 1–42 days. The concentrations (C_i) of Cs and Sr in leachate were analyzed by inductively coupled plasma mass spectrometry (ICP-Mass, Agilent 7700x, Agilent, USA). The normalized leaching rates (NL_i, g·m^{-2}·d^{-1}) of Cs and Sr were calculated as the following equation:

$$\mathrm{NL}_i = \frac{C_\mathrm{i} \cdot V}{\mathrm{SA} \cdot f_\mathrm{i} \cdot t_\mathrm{n}}$$

where C_i (g·m^{-3}) is the concentration of element i = (Cs and Sr) in the leachate, V (m^3) is the volume of the leachate, SA (m^2) is the surface area of leached samples, f_i (wt%) is the mass fraction of element i in the leached ceramics and t_n (days) is the leaching time.

Results and discussion

Phase formation and crystalline structure

Figure 1 shows the TG-DSC curves of the precursor powders used in the synthesis of HP-3 ceramic sample. As shown in the TG-DSC graph, four weight loss stages are distinctly observed from room temperature to 1250 °C. For the first stage from room

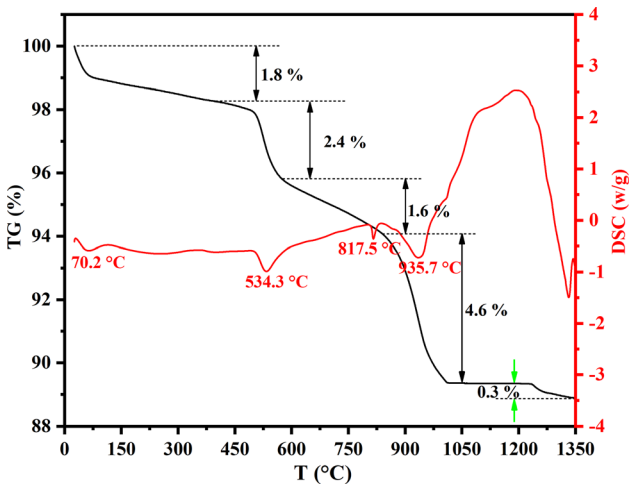

Figure 1 TG-DSC curves of HP-3 powder precursors.

temperature to 400 °C, a mass loss of 1.8% is ascribed to the dehydration physisorbed and chemisorbed water in the precursor powders [31], corresponding to endothermic peak at 70.2 °C in the DSC curve. The second stage with 2.4% mass loss between 400–570 °C could be due to the decomposition of Cs_2CO_3 to Cs_2O, homologizing the endothermic peak at 534.3 °C in the DSC curve [32]. With regard to the third stage between 570 and 840 °C, a weight loss of 1.6% was observed in the TG curve, accompanied by an endothermic peak at 817.5 °C in the DSC curve, which may be assigned to the decomposition of $SrCO_3$ [33]. The last stage with 4.6% mass loss in the range of 840–1020 °C and the endothermic peak at 935.7 °C may be attributed to the decomposition of $BaCO_3$ [34]. Notably, the mass is almost unchanged at 1020–1250 °C, and the DSC curve displays a broad exothermic peak due to the crystallization of hollandite and perovskite phases. This result indicates that the targeted hollandite–perovskite waste form could be synthesized above 1020 °C.

It is well known that elemental Cs and most cesium compounds are volatile at high temperature (> 900 °C). An elevated sintering temperature could lead to a severe Cs loss. As shown in Fig. 1, ~ 0.3% of weight loss is observed at 1250 ~ 1350 °C, indicating a poor Cs retention in sintered sample at elevated temperatures. To explore an optimum sintering temperature, HP-3 powder precursors were sintered at 1200, 1250, 1300 and 1350 °C for 5 h, respectively.

Figure 2a presents the XRD patterns for HP-3 samples sintered at different temperatures (1200, 1250, 1300 and 1350 °C) for 5 h. It is found that the hollandite–perovskite composite ceramics are formed at 1200 °C with small amount of unreacted TiO_2 and the $BaTi_5O_{11}$ metastable intermediate phase [35]. With increasing sintering temperature, the metastable $BaTi_5O_{11}$ phase disappears, indicating an increasing sintering temperature plays a significant role in improving the phase purity of the targeted hollandite–perovskite ceramics. However, after sintering at 1350 °C, TiO_2 phase is still observable in the synthesized sample. The TiO_2 probably originates from excess Ti, due to Cs volatilization at the high temperature [36, 37]. It is worth noting that the peak intensity of TiO_2 phase in the XRD patterns of 1300 °C sintered sample is weaker than that of 1250 and 1350 °C, suggesting a lower TiO_2 content which can be verified by XRD refined compositions. As shown in Fig. 2b-d, the calculated phase compositions demonstrate that the weight fraction of TiO_2 in 1300 °C sintered sample is lower that of 1250 and 1350 °C synthesized samples. This result indicates that the hollandite–perovskite composite ceramics with high phase purity can be considered to fabricating at 1300 °C for 5 h; this was thus selected.

XRD patterns of the sintered hollandite–perovskite ceramics at 1300 °C for 5 h are displayed in Fig. 3. As observed in Fig. 3, all samples are major hollandite and perovskite phases with little of TiO_2, suggesting the desired matrices have been formed.

To further investigate the phase compositions of as-prepared samples at 1300 °C, XRD data are analyzed by the Rietveld method using the GSAS program, the calculated phase compositions and unit-cell parameters are listed in Table 2. From Table 2, the refined results further illuminate that all samples are composed of hollandite, perovskite and TiO_2. In addition, for the targeted hollandite and perovskite matrices, the refined structural parameters fit well with the tetragonal hollandite ($a = b \sim 9.99$ Å, $c \sim 2.92$ Å) and cubic perovskite ($a = b = c \sim 3.91$ Å) phases. This is agreement with powder diffraction data for $Cs_{0.187}Ba_{0.965}Al_{2.115}Ti_{5.885}O_{16}$ (PDF# 78–0018) and $SrTiO_3$ (PDF# 35–0734). Combined with TG-DSC analysis, the schematic of solid-state method for hollandite–perovskite ceramic waste form synthesis is summarized in Fig. 4.

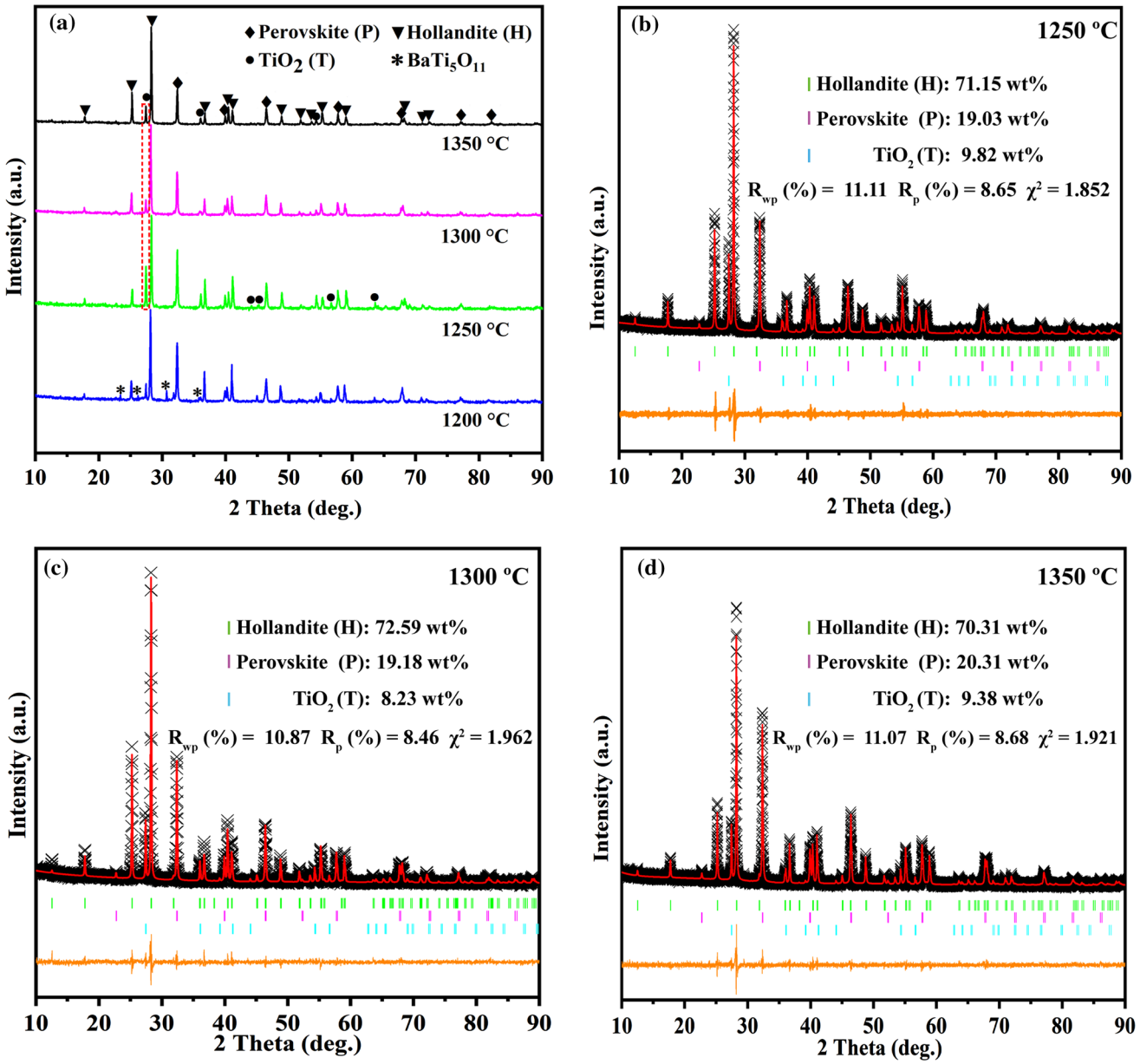

Figure 2 **a** XRD patterns of HP-3 sample sintered at 1200, 1250, 1300 and 1350 °C, (**b-d**) the fitted XRD diffraction pattern of HP-3 sample.

Phase distribution and chemical composition

The phase distribution and chemical composition are identified using BSE-EDX analysis. Figure 5 shows the BSE contrast images and EDX analysis of polished HP-3 ceramic sample. It can be found in Fig. 5a that three contrast discrepancies are clearly observed, indicating these three phases coexist in the as-prepared composite. In addition, these three crystalline phases observed in the BSE image are verified using EDX elemental mapping analysis (Fig. 5b–f). The EDX element mapping collected on different matrices reveals that the "light grey" region is rich in Sr and Ti, "grey" region is rich in Cs, Ba, Al and Ti, while "dark grey" area is only rich in Ti. According to the result of the EDX analysis, it can be confirmed that the light grey, grey and dark grey phases correspond to perovskite, hollandite and TiO_2 matrices respectively, in agreement with above XRD results (Fig. 3).

To investigate the chemical compositions of the targeted hollandite and perovskite matrices in the

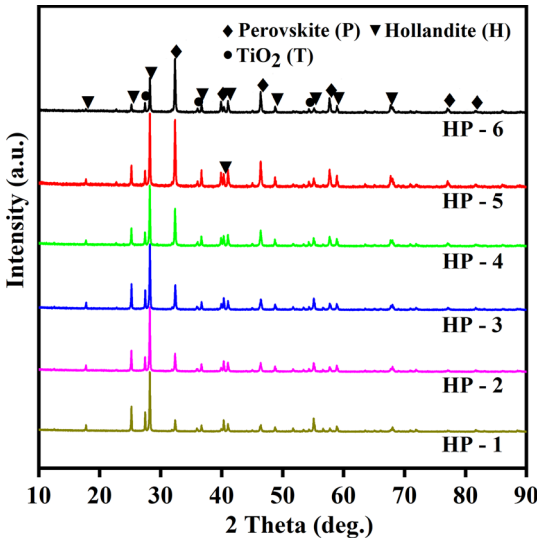

Figure 3 XRD patterns of the HP-1 ~ 6 ceramics sintered at 1300 °C for 5 h.

mixture, the EDX spectra of the selected regions (labeled as "A" and "B" in Fig. 5a) are present in Fig. 5g, h. As seen in EDX spectra, Cs L, Ba L, Ti K, Al K and O K peaks exist in "A" zone while the "B" area contains the peaks of Sr L, Ti K and O K, further confirming the "light grey" matrix is perovskite while the "grey" phase is hollandite. Intriguingly, the calculated formula of perovskite phase in the sample is $Sr_{0.96}Ti_{1.02}O_3$ (Fig. 5h), which is perfectly consistent with the original designed constituent $SrTiO_3$. However, in comparison with Sr-bearing perovskite, Cs-bearing hollandite exhibits an obvious deviation from designed stoichiometry (i.e., $Cs_{0.4}Ba_{0.8}Al_2Ti_6O_{16}$), only ~ 67.5% of the targeted Cs concentration is retained within the prepared hollandite matrix (Fig. 5g). The Cs loss is due to Cs vaporization during sintering, and supported by previous results [38, 39]. It is worth to mention the previous investigations

Table 2 Identified phases and unit-cell parameters of synthetic hollandite–perovskite composite ceramic at 1300 °C ($H = Ba_{0.8}Cs_{0.4}Al_2Ti_6O_{16}$; $P = SrTiO_3$; $T = TiO_2$)

Phase composition		Calculated phase composition			Hollandite		Perovskite	χ^2	R_{wp}	R_p
H	*P*	*H*	*P*	*T*	*a* = *b* (Å)	*c* (Å)	*a* = *b* = *c* (Å)			
85 wt%	15 wt%	80.4 wt%	11.45 wt%	8.15wt%	9.993(0)	2.924(5)	3.907(9)	2.160	12.07%	9.33%
80 wt%	20 wt%	75.75 wt%	16.23 wt%	8.02 wt%	9.985(3)	2.923(4)	3.906(7)	1.998	11.32%	8.84%
75 wt%	25 wt%	72.59 wt%	19.18 wt%	8.23 wt%	9.992(0)	2.924(3)	3.907(7)	1.963	10.87%	8.46%
70 wt%	30 wt%	64.8 wt%	26.68 wt%	8.52 wt%	9.992(0)	2.924(3)	3.909(4)	1.772	10.09%	7.95%
65 wt%	35 wt%	59.86 wt%	31.74 wt%	8.4 wt%	9.987(2)	2.922(3)	3.906(1)	1.797	9.86%	7.78%
60 wt%	40 wt%	55.25 wt%	36.23 wt%	8.52 wt%	9.988(2)	2.924(0)	3.909(0)	1.829	9.76%	7.65%

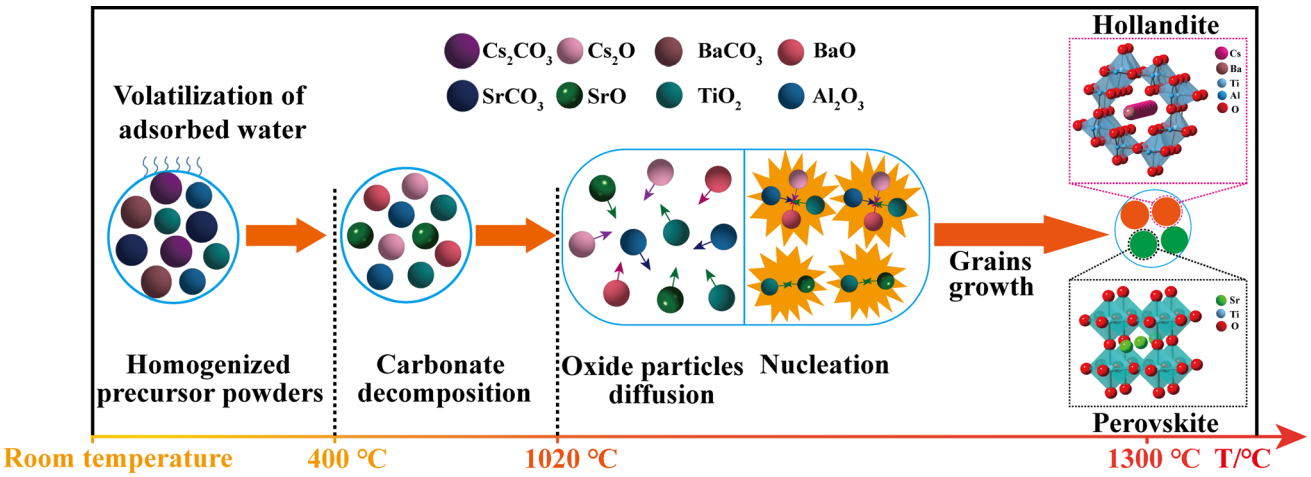

Figure 4 Schematic of the synthesis procedures of hollandite–perovskite ceramics by a solid-state reaction method.

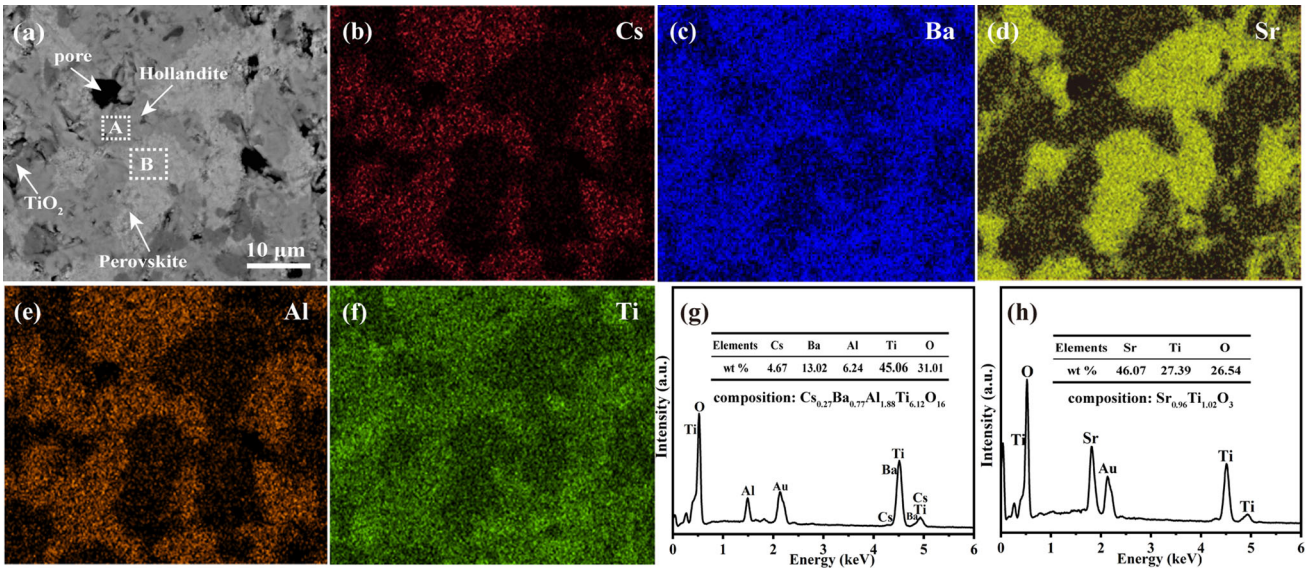

Figure 5 **a** Backscattered electron SEM micrograph of the polished HP-3 sample at 1300 °C, (**b** ∼ **f**) elemental mapping images of Cs, Ba, Al, Sr and Ti, (**g**, **h**) EDX spectra of the labeled two areas (A and B) of **a**.

show the optimum sintering temperature for the (Cs, Ba)-hollandite ceramics is around 1250 °C using high temperature solid-state method [40, 41], thus it is difficulty to improve the Cs retention in our work using the same method. Accordingly, the hot pressed sintering method will be further explored in our next work due to its predominant property with shorter sintering period and lower sintering temperature [42], which may give rise to reduction of cesium volatilization.

Chemical durability

To evaluate the chemical durability of hollandite–perovskite ceramic, MCC-1 is performed on the selected HP-3 composition. The normalized release rates of Cs and Sr in HP-3 sample are measured over a 42-day period, and the results are shown in Fig. 6. It can be seen in Fig. 6 that the normalized leaching rates of Cs and Sr decrease rapidly during the 14-day test period and slowly decrease with increasing time, then remain nearly constant after 14 days. This result indicates that the leaching behavior of Cs and Sr in hollandite–perovskite ceramics can be explained by the interfacial dissolution-re-precipitation mechanism [43, 44]. It should be noted that, after 42 days leaching, the calculated NL_{Cs} and NL_{Sr} in the HP-3 sample (5.2 wt.% cesium + 16.9 wt.% strontium waste loading on an oxide basis) are respectively 7.83×10^{-3} g·m^{-2}·d^{-1} and 4.32×10^{-5} g·m^{-2}·d^{-1}, which is lower than that of $10^{-1} \sim 10$ g·m^{-2}·d^{-1} in the borosilicate glass waste form with 1.09 wt.% cesium oxide and 0.40 wt.% strontium oxide loading [15, 30]. Moreover, the obtained data are also slightly lower than the reported values of $\sim 10^{-2}$ g·m^{-2}·d^{-1} for Cs and Sr in synroc-C [45], exhibiting an excellent leaching resistance to Cs and Sr.

Figure 7 presents SEM–EDS images and XRD patterns of the prepared sample before and after leaching. It can be seen from Fig. 7a that the pre-leaching sample possesses a smooth and clean surface morphology, while some floccules are observed on surface of post-leaching sample after leaching 42 days (Fig. 7b). The observed floccules could be ascribed to the formation of precipitates with respect to the released ionic species [46]. However, the precipitate phases fail to be determined by EDS and XRD, owing to their contents below the instrumental detection limit [10, 47]. As observed in Fig. 7c, the elemental mapping analysis reveals the homogeneous distribution of Cs Ba, Al, and Ti in the "H" zone and the Sr and Ti are distributed uniformly throughout the "P" area. Importantly, the EDS analysis indicates that the chemical compositions of hollandite matrix is well agreement between the pre-leaching and post-leaching HP-3 samples (Figs. 5g and 7d), as well as perovskite host (Figs. 5h and Fig. 7e). Furthermore, the additional peaks are not observed in the post-leaching sample in the XRD patterns, in accordance with the previous results [48]. It confirms that the aqueous

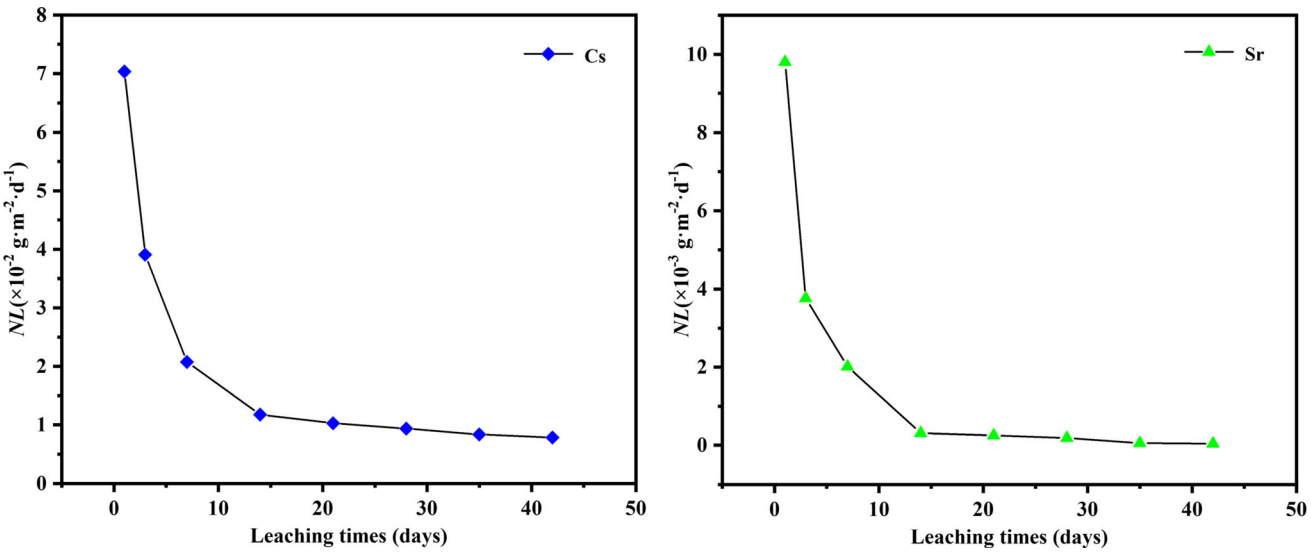

Figure 6 Normalized release rates of Cs and Sr in the HP-3 ceramics waste forms.

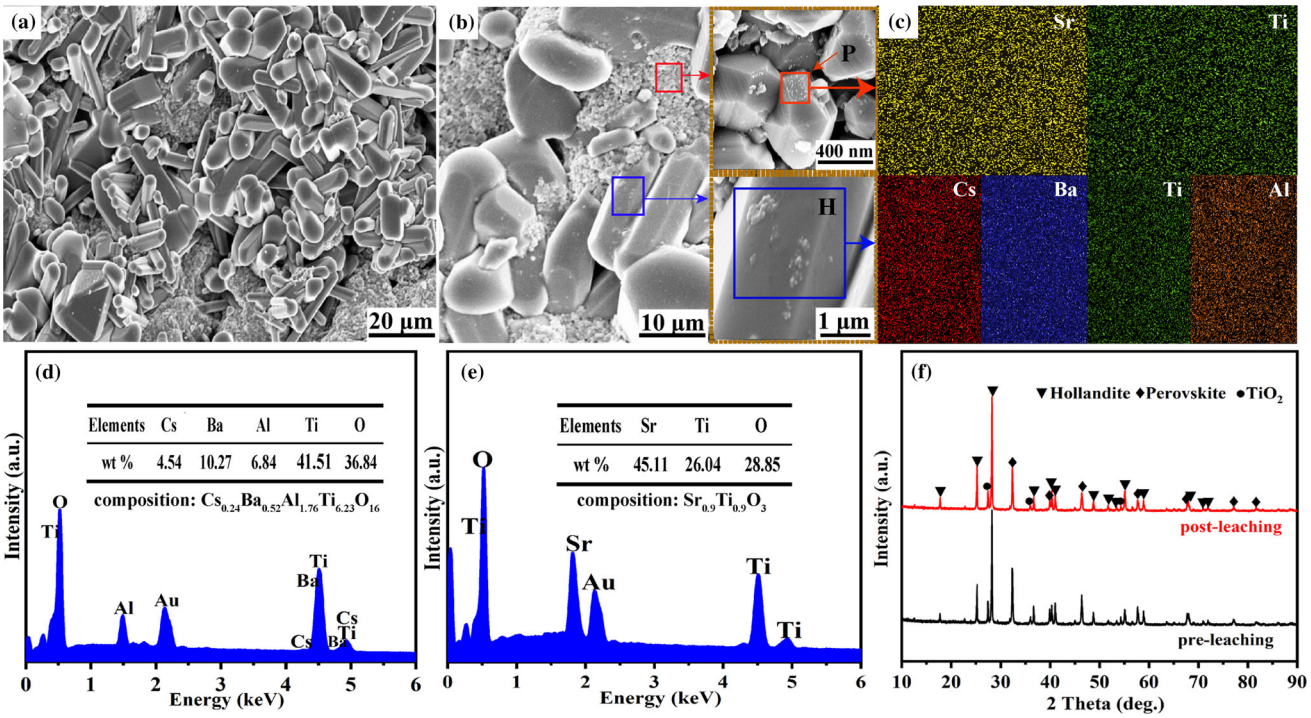

Figure 7 **a** SEM image before leaching, **b** SEM image after leaching for 42 days, **c** corresponding elemental mapping images of P and H zones in the **b**, (**d**, **e**) EDS spectra of the labeled two areas (H and P) of **b**, **f** XRD patterns of HP-3 ceramic waste form before and after leaching.

corrosion does not induce substantial structural changes of the Cs- and Sr-bearing hosts. Therefore, hollandite–perovskite ceramics are considered as a promising waste form for safety immobilization of the separated Cs and Sr from HLW streams.

Conclusions

In the present study, a hollandite–perovskite ceramic matrix is considered as a promising host matrix for Cs and Sr immobilization. The phase composition, crystal structure and chemical durability of the

synthesized composites are investigated. The results show that hollandite and perovskite are the major phases in the all samples along with a small amount of TiO_2. Moreover, Cs-bearing hollandite matrix shows a tetragonal structure ($I4/m$) while Sr-bearing perovskite exhibits a cubic structure ($Pm\ \bar{3}m$). The 42 days normalized leaching rates of Cs and Sr were measured to be 7.83×10^{-3} g·m^{-2}·d^{-1} and 4.32×10^{-5} g·m^{-2}·d^{-1}, respectively. Moreover, the aqueous corrosion does not induce substantial structural changes of Cs/Sr-bearing hosts. These results suggest that the hollandite–perovskite waste form is a promising candidate to safely immobilize the separated Cs and Sr waste stream from HLW.

Acknowledgements

We sincerely acknowledge the financial support from the National Natural Science Foundation of China (Grant Nos. 41574100, 11705152).

Compliance with ethical standards

Conflict of interest The authors declare no conflict of interest

References

[1] Ewing RC, Whittleston RA, Yardley BW (2016) Geological disposal of nuclear waste: a primer. Elements 12:233–237. https://doi.org/10.2113/gselements.12.4.233

[2] Dhara A, Mishra RK, Shukla R, Valsala TP, Sudarsan V, Tyagi AK, Kaushik CP (2016) A comparative study on the structural aspects of sodium borosilicate glasses and barium borosilicate glasses: effect of Al_2O_3 addition. J Non Cryst Solids 447:283–289. https://doi.org/10.1016/j.jnoncrysol.2016.04.040

[3] Goel A, McCloy JS, Pokorny R, Kruger AA (2019) Challenges with vitrification of hanford high-level waste (HLW) to borosilicate glass: an overview. J Non Cryst Solids X 4:100033 (1-19). https://doi.org/10.1016/j.nocx.2019.100033

[4] Salvatores M, Palmiotti G (2011) Radioactive waste partitioning and transmutation within advanced fuel cycles: achievements and challenges. Prog Part Nucl Phys 66:144–166. https://doi.org/10.1016/j.ppnp.2010.10.001

[5] McMaster SA, Ram R, Faris N, Pownceby MI (2018) Radionuclide disposal using the pyrochlore supergroup of minerals as a host matrix: a review. J Hazard Mater 360:257–269. https://doi.org/10.1016/j.jhazmat.2018.08.037

[6] Beswick AJ, Gibb FGF, Travis KP (2014) Deep borehole disposal of nuclear waste: engineering challenges. Proc Inst Civil Eng Energy 167:47–66. https://doi.org/10.1680/ener.13.00016

[7] Ojovan MI, Lee WE (2011) Glassy wasteforms for nuclear waste immobilization. Metall Mater Trans A 42:837–851. https://doi.org/10.1007/s11661-010-0525-7

[8] Gin S, Jollivet P, Tribet M, Peuget S, Schuller S (2017) Radionuclides containment in nuclear glasses: an overview. Radiochim Acta 105:927–959. https://doi.org/10.1515/ract-2016-2658

[9] Ringwood AE, Oversby VM, Kesson SE, Sinclair W, Ware N, Hibberson W, Major A (1981) Immobilization of high-level nuclear reactor wastes in synroc: a current appraisal. Nucl Chem Waste Manag 2:287–305. https://doi.org/10.1016/0191-815X(81)90055-3

[10] Meng C, Li W, Ren C, Zhao J (2020) Structure and chemical durability studies of powellite ceramics $Ca_{1-x}Li_{x/2}$ $Gd_{x/2}MoO_4$ ($0 \le x \le 1$) for radioactive waste storage. J Mater Sci 55:2741–2749. https://doi.org/10.1007/s10853-019-04223-y

[11] Hsieh YH, Rushton MJD, Fossati PCM, Lee WE (2020) Thermal footprint of a geological disposal facility containing EURO-GANEX wasteforms. Prog Nucl Energy 118:103065. https://doi.org/10.1016/j.pnucene.2019.103065

[12] Wang L, Liang T (2012) Ceramics for high level radioactive waste solidification. J Adv Ceram 1:194–203. https://doi.org/10.1007/s40145-012-0019-8

[13] Ravikumar R, Gopal B, Jena H (2020) Fabrication, chemical and thermal stability studies of crystalline ceramic waste-form based on oxyapatite phosphate host $LaSr_4(PO_4)_3O$ for high level nuclear waste immobilization. J Hazard Mater 394:122552. https://doi.org/10.1016/j.jhazmat.2020.122552

[14] Orlova AI, Ojovan MI (2019) Ceramic mineral waste-forms for nuclear waste immobilization. Materials 12:2638. https://doi.org/10.3390/ma12162638

[15] Stefanovsky SV, Yudintsev SV, Gieré R, Lumpkin GR (2004) Nuclear waste forms. Geol Soc Lond Spec Publ 236:37–63. https://doi.org/10.1144/GSL.SP.2004.236.01.04

[16] Luo S, Li L, Tang B, Wang D (1998) Synroc immobilization of high level waste (HLW) bearing a high content of sodium. Waste Manag 18:55–59. https://doi.org/10.1016/S0956-053X(97)00019-6

[17] Newkirk H, Ryerson F, Coles D, Hoenig C, Rozsa R, Rossington C, Bazan F, Tewhey J (1980). Phase equilibria, leaching characteristics and ceramic processing of SYNROC D formulations for US defense wastes (No. UCRL-85483;

CONF-801124–45). California Univ, Livermore (USA) Lawrence Livermore National Lab

[18] Hambley MJ, Dumbill S, Maddrell ER, Scales CR (2008) Characterisation of 20 year old ^{238}Pu-doped Synroc C (conference paper). Mater Res Soc Symp Proc 1107:373–380. https://doi.org/10.1557/PROC-1107-373

[19] Chao X, Wang J, Chen J (2012) Solvent extraction of strontium and cesium: a review of recent progress. Solvent Extr Ion Exc 30:623–650. https://doi.org/10.1080/07366299.2012.700579

[20] Sengupta P, Sanwal J, Mathi P, Mondal JA, Mahadik P, Dudwadkar N, Gandhi PM (2017) Sorption of Cs and Sr radionuclides within natural carbonates. J Radioanal Nucl Chem 312:19–28. https://doi.org/10.1007/s10967-017-5206-1

[21] Dozol JF, Dozol M, Macias RM (2000) Extraction of strontium and cesium by dicarbollides, crown ethers and functionalized calixarenes. J Incl Phenom Macro 38:1–22. https://doi.org/10.1023/A:1008145814521

[22] Mimura H, Akiba K, Igarshi H (1993) Removal of heat-generating nuclides from high-level liquid wastes through mixed zeolite columns. J Nucl Sci Technol 30:239–247. https://doi.org/10.1080/18811248.1993.9734476

[23] Tumurugoti P, Clark BM, Edwards DJ, Amoroso J, Sundaram SK (2017) Cesium incorporation in hollandite-rich multiphasic ceramic waste forms. J Solid State Chem 246:107–112. https://doi.org/10.1016/j.jssc.2016.11.007

[24] Xu H, Wu L, Zhu J, Navrotsky A (2015) Synthesis, characterization and thermochemistry of Cs-, Rb- and Sr- substituted barium aluminium titanate hollandites. J Nucl Mater 459:70–76. https://doi.org/10.1016/j.jnucmat.2015.01.014

[25] Navi NU, Shneck RZ, Shvareva TY, Kimmel G, Zabicky J, Mintz MH, Navrotsky A (2012) Thermochemistry of $(Ca_{x}Sr_{1-x})TiO_3$, $(Ba_xSr_{1-x})TiO_3$, and $(Ba_xCa_{1-x})TiO_3$ perovskite solid solutions. J Am Ceram Soc 95:1717–1726. https://doi.org/10.1111/j.1551-2916.2012.05137.x

[26] Bailey DJ, Stennett MC, Mason AR, Hyatt NC (2018) Synthesis and characterisation of the hollandite solid solution $Ba_{1.2-x}Cs_xFe_{2.4-x}Ti_{5.6+x}O_{16}$ for partitioning and conditioning of radiocaesium. J Nucl Mater 503:164–170. https://doi.org/10.1016/j.jnucmat.2018.03.005

[27] Levy MR, Steel BC, Grimes RW (2004) Divalent cation solution in $A3^{+}B^{3+}O_3$ perovskites. Solid State Ionics 175:349–352. https://doi.org/10.1016/j.ssi.2004.02.072

[28] Maddrell E (2013) Hot isostatically pressed waste forms for future nuclear fuel cycles. Chem Eng Res Des 91:735–741. https://doi.org/10.1016/j.cherd.2012.11.004

[29] Toby BH (2001) EXPGUI, a graphical user interface for GSAS. J Appl Crystallogr 34:210–213

[30] Strachan DM, Turcotte RP, Barnes BO (1982) MCC-1: a standard leach test for nuclear waste forms. Nucl Technol 56:306–312. https://doi.org/10.13182/NT82-A32859

[31] Feng T, Li L, Lv Z, Li B, Zhang Y, Li G (2019) Temperature-dependent electrical transport behavior and structural evolution in hollandite-type titanium-based oxide. J Am Ceram Soc 102:6741–6750. https://doi.org/10.1111/jace.16520

[32] Wang X, Ma J, Lu X, Fang Z, Li L, Li L, Yang Y (2020) Investigations on the structural evolution and aqueous durability of $[Cs_xBa_y][Fe^{3+}_{2y+x}Ti^{4+}_{8-2y-x}]O_{16}$ ceramics for radioactive cesium storage. J Solid State Chem 288:121457. https://doi.org/10.1016/j.jssc.2020.121457

[33] Luxová J, Šulcová P, Trojan M (2008) Study of perovskite compounds. J Therm Anal Calorim 93:823–827. https://doi.org/10.1007/s10973-008-9329-z

[34] Grote R, Zhao M, Shuller-Nickles L, Amoroso J, Gong W, Lilova K, Brinkman KS (2019) Compositional control of tunnel features in hollandite-based ceramics: structure and stability of (Ba, $Cs)_{1.3}3(Zn, T_i)_{8O}16$. J Mater Sci 54:1112–1125. https://doi.org/10.1007/s10853-018-2904-1

[35] Grigor'eva LF, Petrov SA, Sinel'shchikova OY, Gusarov VV (2003) Mechanism of the formation of $Ba_2Ti_9O_{20}$-based phases in the course of solid-phase interaction in the BaO-$TiO_2(ZrO_2)$ and Cs_2O-BaO-$TiO_2(ZrO_2)$ systems. Glass Phys Chem 29:188–193. https://doi.org/10.1023/A:1023415327336

[36] Amoroso JW, Marra J, Dandeneau CS, Brinkman K, Xu Y, Tang M, Maio V, Webb SM, Chiu WKS (2017) Cold crucible induction melter test for crystalline ceramic waste form fabrication: a feasibility assessment. J Nucl Mater 486:283–297. https://doi.org/10.1016/j.jnucmat.2017.01.028

[37] Zhao MY, Russell P, Amoroso J, Misture S, Utlak S, Besmann T, Nickles LS, Brinkman KS (2020) Exploring the links between crystal chemistry, cesium retention, thermochemistry and chemical durability in single-phase (Ba, $Cs)_{1.33}(Fe, T_i)_8O_{16}$ hollandite. J Mater Sci 55:6401–6416. https://doi.org/10.1007/s10853-020-04447-3

[38] Amoroso J, Marra J, Conradson SD, Tang M, Brinkman K (2014) Melt processed single phase hollandite waste forms for nuclear waste immobilization: $Ba_{1.0}Cs_{0.3}A_{2.3}Ti_{5.7}O_{16}$; A = Cr, Fe. Al J Alloy Compd 584:590–599. https://doi.org/10.1016/j.jallcom.2013.09.087

[39] Xu Y, Wen Y, Grote R, Amoroso J, Nickles LS, Brinkman KS (2016) A-site compositional effects in Ga-doped hollandite materials of the form $Ba_xCs_yGa_{2x+y}Ti_{8-2x-y}O_{16}$: implications for Cs immobilization in crystalline ceramic waste forms. Sci Rep 6:27412. https://doi.org/10.1038/srep27412

[40] Leinekugel-le-Cocq AY, Deniard P, Jobic S, Cerny R, Bart F, Emerich H (2006) Synthesis and characterization of hollandite-type material intended for the specific containment of radioactive cesium. J Solid State Chem 179:3196–3208. https://doi.org/10.1016/j.jssc.2006.05.047

[41] Yang Y, Wang X, Luo S, Yang X, Ma J (2019) Stability studies of $[Cs_xBa_y][(Al^{3+}, T^{i3+})_{2y+x}T^{i4+}_{8-2y-x}]O_{16}$ ceramics for radioactive caesium immobilization. Ceram Int 45:7865–7870. https://doi.org/10.1016/j.ceramint.2019.01.095

[42] Bailey DJ, Stennett MC, Hyatt NC (2020) $Ba_{1.2-x}Cs_xM_{1.2-x/2}Ti_{6.8+x/2}O_{16}$ (M = Ni, Zn) hollandites for the immobilisation of radiocaesium. MRS Adv 5:55–64. https://doi.org/10.1557/adv.2020.43

[43] Danelska A, Ulkowska U, Socha RP, Szafran M (2013) Surface properties of nanozirconia and their effect on its rheological behaviour and sinterability. J Eur Ceram Soc 33:1875–1883. https://doi.org/10.1016/j.jeurceramsoc.2013.01.019

[44] Tang Y, Shih K (2015) Mechanisms of zinc incorporation in aluminosilicate crystalline structures and the leaching behaviour of product phases. Environ Technol 36:2977–2986. https://doi.org/10.1080/09593330.2014.982715

[45] Gregg DJ, Farzana R, Dayal P, Holmes R, Triani G (2020) Synroc technology: perspectives and current status. J Am Ceram Soc 103:5424–5441. https://doi.org/10.1111/jace.17322

[46] Luca V, Cassidy D, Drabarek E, Murray K, Moubaraki B (2005) Cesium extraction from $Cs_{0.8}Ba_{0.4}Ti_8O_{16}$ hollandite nuclear waste form ceramics in nitric acid solutions. J Mater Res 20:1436–1446. https://doi.org/10.1557/JMR.2005.0204

[47] Kumar SP, Gopal B (2015) Simulated monazite crystalline wasteform $La_{0.4}Nd_{0.1}Y_{0.1}Gd_{0.1}Sm_{0.1}Ce_{0.1}Ca_{0.1}(P_{0.9}Mo_{0.1}O_4)$: synthesis, phase stability and chemical durability study. J Nucl Mater 458:224–232. https://doi.org/10.1016/j.jnucmat.2014.12.081

[48] Li WQ, Ding XG, Meng C, Ren CR, Wu HT, Yang H (2018) Phase structure evolution and chemical durability studies of $Gd_{1-x}Yb_xPO_4$ ceramics for immobilization of minor actinides. J Mater Sci 53:6366–6377. https://doi.org/10.1007/s10853-018-2031-z